NUCL SCI TECH (2020) 31:18
https://doi.org/10.1007/s41365-020-0723-y

Comparison of time-related electrical properties of PN junctions and Schottky diodes for ZnO-based betavoltaic batteries

Xiao-Yi Li[1] · Jing-Bin Lu[1] · Ren-Zhou Zheng[1] · Yu Wang[1] · Xu Xu[1] · Yu-Min Liu[2] · Rui He[1]

Received: 10 October 2019 / Revised: 4 December 2019 / Accepted: 16 December 2019 / Published online: 3 February 2020

Abstract Schottky diodes and PN junctions were utilized as energy converting structures in ZnO-based betavoltaic batteries, in which 0.101121 Ci ^{63}Ni was selected as the beta source. The time-related electrical properties were obtained using Monte Carlo simulations. For the n-type ZnO, the Pt/ZnO Schottky diode had the highest energy conversion efficiency, and the Ni/ZnO Schottky diode had the largest I_{sc}. The overall electrical performance of PN junctions is better than that of Schottky diodes. The lifetimes of Pt/ZnO and Ni/ZnO are longer than for other Schottky devices, coming close to those of PN junctions. Considering that Schottky diodes are easier to fabricate and independent of p-type semiconductors, Pt/ZnO and Ni/ZnO diodes offer alternatives to PN-junction-based betavoltaic batteries.

Keywords Beta voltaic effect · Zinc oxide · Time-related properties · PN junction · Schottky diode · Monte Carlo simulation

This work was supported by the National Major Scientific Instruments and Equipment Development Projects (No. 2012YQ240121) and National Natural Science Foundation of China (No. 11075064).

✉ Jing-Bin Lu
ljb@jlu.edu.cn

[1] College of Physics, Jilin University, Changchun 130012, China

[2] East China University of Technology, Nanchang 330013, China

1 Introduction

MEMS (microelectromechanical systems) is a fabrication technology by which a microfabricated miniature electromechanical structure can be added to an integrated circuit (IC) [1]. These devices have both mechanical and electronic parts, with size ranging from a few micrometers to millimeters. Their functions include sensing, control, and execution at microscale and have the ability to impact macroscopic domains [2]. However, the conventional power supplies used with MEMS have disadvantages. For example, chemical batteries have low energy density and short lifetime, solar cells cannot work properly in conditions without steady illumination [3], and fuel cells or other devices using fossil fuels, must replenish the liquid fuel supply while eliminating byproducts formed inside the electronics [4]. Under these conditions, nuclear microbatteries, especially betavoltaic batteries, have become promising candidates to supply power to MEMS. A nuclear battery has very high energy density (the total energy content per unit mass): approximately 10^2 to 10^4 times higher than that of chemical or fossil fuels [5], while the power density is lower than that of conventional batteries. Based on semiconductor technology, some kinds of nuclear batteries can be miniaturized and integrated easily. Considering the long lifetimes of isotopes, and the spontaneity and stability of the decay process, such batteries can serve well under extreme conditions for many years. Generally, the domains of operation of a nuclear battery include long duration, no maintenance, low power, and high-energy power supply.

The first nuclear battery was made by Mosely in 1913, which directly used the charges of beta particles (electrons) to derive a current [6]. Subsequently, the first study of a

betavoltaic battery was conducted in 1951, by Ehrenberg [7]. This was followed by the first betavoltaic battery (fabricated by Rappaport in 1953) using $^{90}Sr/^{90}Y$ with a semiconductor junction. The efficiency obtained was 0.4% [8]. Since the 1960s, several experiments involving betavoltaic batteries have been carried out, some of which were used in pacemakers [9, 10]. However, considering the high cost and the toxicity of the contaminating isotope ^{146}Pm, the nuclear batteries used in pacemakers were replaced with safer lithium-ion batteries [11]. In the 1990s, due to the continuous development of MEMS, betavoltaic batteries eventually became a major alternative among micropower sources. Various radioisotopes, semiconductors, and energy converting structures have been simulated and tested to gain additional output power. The candidate isotopes include ^{147}Pm [9], ^{35}S [12], ^{3}H [13], ^{63}Ni [3, 14], ^{90}Sr [11], and ^{14}C [15]. The two main energy converting structures are PN junctions and Schottky devices. With a planar conversion structure, a large portion of the energy is wasted because of the angular distribution of emitted particles. Therefore, a nonplanar structure is utilized to increase the contact area between the source and the energy converting portion. This has enabled the use of additional energy [16]. More recently, betavoltaic batteries with nanostructures have also been proposed. One of these batteries uses one-dimensional ZnO nanowires, and by applying a sandwich structure, the betavoltaic device achieved excellent electrical performance. With a source radiating 10 mCi $^{63}Ni/Ni$, the open-circuit voltage, short-circuit current, and effective energy conversion efficiency were 2.74 V, 18.4 nA, and 27.92%, respectively [17].

The development of the semiconductor industry has also played an important role in promoting betavoltaic battery research. In the 1950s, although Si was the first candidate energy converting material because of its technical maturity, its conversion efficiency was relatively low and it was vulnerable to radiation damage (the radiation threshold is $\sim$ 200–250 keV; see [18]). Since then, a variety of semiconductors have been extensively researched. One of the main research achievements is the determination that the limit of conversion efficiency is a function of the bandgap [19]; specifically, that a betavoltaic battery using wide-bandgap semiconductors has higher conversion efficiency. Meanwhile, the open-circuit voltage and short-circuit current have also become higher, and new conductors are more radiation tolerant [20]. Consequently, third-generation semiconductors have become the focus of more recent research. SiC [3, 20–22] and GaN [23, 24], in particular, are the most popular objects of research utilizing both Monte Carlo simulation and experimental methods. However, the growth of both materials is expensive and occurs at high temperature; therefore, a lower-cost semiconductor is preferred. Until now, there have been many studies about PN junction or Schottky diode-based betavoltaic batteries individually, but studies comparing electrical properties using these two structures on the same semiconductor are very few. Tarelkin et al. compared different metals in a Schottky barrier betavoltaic battery [25] and Rahmani compared Si-based PN junctions and Ni/Si Schottky barriers [26]. The performance of Schottky diodes is determined by the properties of the metal and the semiconductor; therefore, to obtain an extensive view of the comparison, the Schottky contact should be formed using the same semiconductor with different metals. Thereafter, different Schottky diodes and PN junctions can be comparable. Unfortunately, such an extended comparison is still lacking. For an advanced material, the doping method may not be mature enough, but this comparison is necessary to determine the potential performance of different devices and to find the best possible technology for fabricating betavoltaic batteries. Moreover, although it is well known that radioisotopes decay incessantly, the influence of time on the performance of betavoltaic batteries has not been explored. In fact, the decay process impacts the electrical performance profoundly, especially for isotopes with gaseous products (i.e., ^{3}H), cascade decays (i.e., ^{90}Sr-^{90}Y), obvious density changes (i.e., ^{147}Pm), or short lifetimes (i.e., ^{35}S). In this paper, a cost-effective third-generation (i.e., wide-bandgap) semiconductor (ZnO) was utilized as the energy converting material of a betavoltaic battery. PN junctions and Schottky diodes with different metals were also used as energy converting structures, and ^{63}Ni was selected as the beta source. To utilize fully the energy produced, the doping concentrations were modulated to match the depletion width and energy deposition range. According to the decay formula of ^{63}Ni, we analyzed the factors that influence the self-absorption effect and energy deposition. Using the Monte Carlo method, the time-related self-absorption process of the source and energy depositions was explored. Finally, the time-related electrical properties for all the devices designed in this work were obtained and compared.

2 Research status on the properties and fabrication of ZnO devices

ZnO is a material with great potential for use in the semiconductor industry. It is a direct bandgap semiconductor with a wide gap (3.37 eV) and is among the third-generation semiconductors (with SiC and GaN). Because of its excellent properties, it has been applied as a piezoelectric material, in varistors, transmittance conductive oxide film, fluorescent material, and in many other applications [27]. The direct and wide bandgap enables optoelectronic applications in the blue/UV region, and for

excitonic-effects-based optical devices, its high exciton binding energy makes it a favorable candidate. In comparison with GaN, the growth of ZnO is much easier. The large and high-quality ZnO bulk substrate is commercially available [28]. Moreover, by applying the homoepitaxial growth method, ZnO can be grown on native substrates, which can reduce the defect concentration and enhance film quality. In contrast, for GaN there are no native substrates. This means that a ZnO-based device of high quality could surpass the efficiencies obtained using GaN-based devices. Moreover, ZnO can be grown at much lower temperature, and the wet chemical etching method is available for it, which mean that the processing, design, and integration of electronic and optoelectronic devices would be more flexible [29]. For a betavoltaic battery, the conversion structure must work for a long time in radiation; therefore, the radiation resistance of a material is of great importance. In fact, radiation damage is one of the major factors leading to degradation of betavoltaic batteries [30, 31], but the extraordinary radiation hardness of ZnO can meet this challenge easily. Under bombardment from high-energy electron flux, no permanent defects are formed in the ZnO lattice [27], which result surpasses those with other common semiconductor materials, including Si, GaAs, CdS, and GaN. This indicates that ZnO devices would be very suitable for space applications [27, 29]. In addition, ZnO is inexpensive, nontoxic, has high breakdown strength, and good chemical stability, which make it a favorable semiconductor for use in radiation tolerant electronics [28].

Two electronic devices important for betavoltaic batteries are PN junctions and Schottky diodes, of which the former has been thoroughly researched. The devices used as the energy converting structure of a nuclear battery should have high performance and long-term stability because they would operate for a long time in radiation. Often, wide-bandgap semiconductors suffer from doping asymmetry problems, which means that a semiconductor can be doped to achieve one type easily, but to obtain a contrary type is rather difficult. ZnO can easily be doped to achieve n-type, but creation of p-type ZnO has remained a challenge for years. In spite of many difficulties, researchers have succeeded in using various dopants and different growth techniques to grow p-type ZnO and even a ZnO homojunction. All these achievements now make it possible to fabricate ZnO-based betavoltaic batteries [32]. Moreover, the fabrication of ZnO homojunction diodes has also evolved in positive ways, adding to the potential for fabricating ZnO-based nuclear batteries. At present, well-maintained p-type ZnO films show no obvious degradation after a year [33]. By adding ZnMgO asymmetric double barriers, the homojunction performance can be enhanced substantially [34, 35]. A series of novel and simpler fabrication methods have also been reported recently. By employing a surface pulsed laser irradiation method, p- and n-type ZnO can be fabricated with only one dopant in a single layer of NZO film [36]. A simple and controllable method at low temperature and in aqueous solution was also put forward, to create an Sb-doped ZnO (SZO)/ZnO film-based homojunction [37]. The wet chemistry method has also been utilized to fabricate ZnO homojunctions that show high rectification ratios [38].

In the mid-1960s, the study of ZnO Schottky contacts was initiated. In comparison with ZnO homojunctions, the research on understanding and control of Schottky contacts on ZnO are relatively mature, especially for n-type ZnO. Experimental results show that Au, Ir, Pt, Pd, and Ag are the main metals used to provide Schottky contact on n-type ZnO, and the Schottky barrier height and ideality factor varies with different chemical treatments on a surface. The Schottky barrier height and ideality factor are usually within the range 0.4–1.2 eV and 1.0–3.57, respectively. Ideally, to get clean ZnO-metal contacts, the surfaces should be prepared under clean conditions. However, for a long time, several studies had not considered this; hence, the reported barrier heights were inconsistent. Even now, there is still no predictable method [39]. For p-type ZnO, Pd is suitable to form a Schottky contact [40], but generally, this research is still in its infancy. In short, ZnO has definite potential as a commendable energy converting material for use in betavoltaic batteries.

3 Principles for the use of Schottky devices and PN junctions in betavoltaic batteries

Schematic diagrams of PN junction and Schottky device-based betavoltaic batteries are shown in Fig. 1. PN junctions play an extremely important role in electronic and optical applications. By joining together n- and p-type semiconductors, a PN junction is formed at the interface. Because of the existence of a concentration gradient, electrons diffuse into the p-region and holes diffuse into the n-region. An electric field that counteracts the diffusion can be created and this electric field can also sweep away mobile charges and obtain a space-charge region [41]. The movable charge carriers can hardly exist in this region; hence, this region is referred to as the depletion region. In fabricating semiconductor devices, there are metallization techniques by which to form Schottky and Ohmic contacts. A Schottky contact is formed using a metal and a semiconductor, and has a rectifying function similar to that of a PN junction [42]. By selecting the proper metals and doping concentration, a potential energy barrier between metal and semiconductor can be formed, analogous to that of a PN junction.

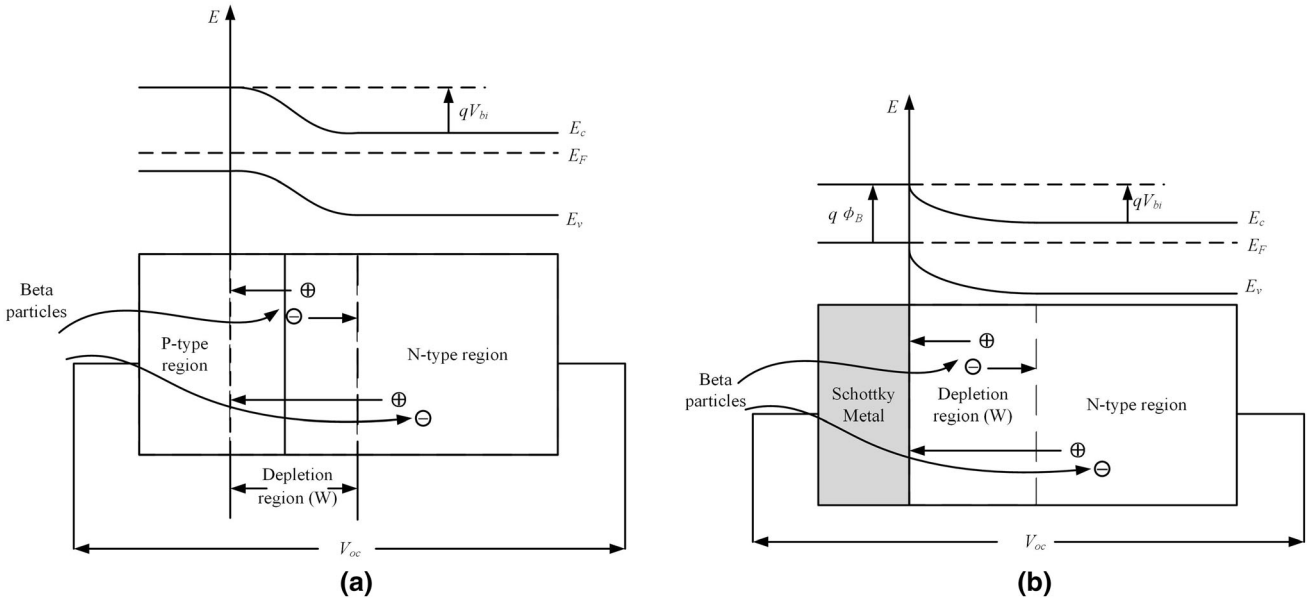

Fig. 1 Schematic diagrams of betavoltaic batteries: **a** PN junction-based and **b** Schottky device-based

When beta particles are emitted into a semiconductor, their energy will produce electron–hole pairs by ionization or transform the energy to heat. Electron–hole pairs can be produced either inside or outside the depletion region. In the depletion region, there is an electrical field that can separate electron–hole pairs, after which the charge carriers will be driven to produce current. However, outside the depletion region, there are no electrical fields to separate the electron–hole pairs, and instead, most of the charge carriers will recombine or become trapped by defects. Some charge carriers can drift into the depletion region, where they become part of the cell current [43].

4 Choice of isotope and corresponding time-related behavior

Usually pure beta emitters are utilized for betavoltaic batteries, because beta particles are easier to shield than is gamma radiation; thus, the most common isotopes considered are ^{3}H, ^{35}S, ^{63}Ni, ^{147}Pm, and ^{90}Sr. Among these isotopes, gaseous ^{3}H is inconvenient to store and load, and its energy is relatively low (average β energy 5.682 keV). The ^{147}Pm source has relatively short half-life (approximately 2.62 a), which is unsuited to long-term, no-refill situations. Moreover, the ^{147}Pm used in betavoltaic batteries usually contains the impurity ^{146}Pm, which is toxic and emits energetic gamma rays (0.75 MeV). The half-life of ^{35}S is only 87.37 d, even shorter than that of ^{147}Pm. The strontium isotope (^{90}Sr) and its product ^{90}Y emit high-energy beta particles (average β energy: 195.8 keV for ^{90}Sr and 933.7 keV for ^{90}Y). However, to utilize fully the energy released, the device would have to be large and would undergo serious radiation damage. For these reasons, ^{63}Ni is preferred for its solid-state, moderate energy (average β energy 17.425 keV), and relatively long half-life (101.2 a). However, for an actual solid-state source, the beta particles can be absorbed by the source itself (the self-absorption effect), which is inevitable. This effect may cause a rise in temperature, energy waste, and performance degradation. Moreover, the source decays continuously, which results in decrease of the radioactivity and changes the components in the source. Consequently, the regular pattern of the self-absorption effect is also changed. By choosing the proper level of radioactivity, the self-absorption effect can be reduced. In this work, the impact of time on the self-absorption effect was also taken into consideration.

The MCNP5 code was utilized in this work, and the number of particles in all the simulating processes was 10^7. In this simulation, a 1 × 1 cm rectangular source with changeable height was used as the energy depositing model, and the self-absorption rate η was defined as:

$$\eta = \frac{P_{\text{in}}}{P_{\text{total}}}, \tag{1}$$

where P_{in} is the deposition power in the source, and P_{total} is the total power. Figure 2a depicts the surface radioactivity and self-absorption rate at initiation, in relation to thickness. With increasing thickness of the source, there is less increase in the surface power, while the self-absorption rate can be very high (approaching 100%). This means that the extra thickness of the source makes no contribution to increase in the surface power. At 2.00337 μm, the surface

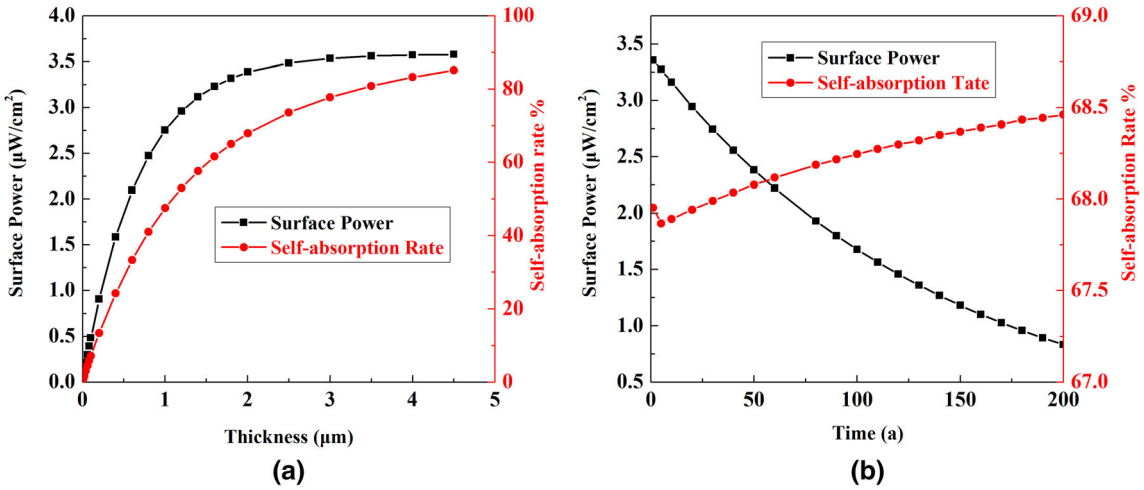

Fig. 2 Time-related self-absorption rate changes: **a** initial and **b** in 200 years (Color online)

power is almost unchanged, and the self-absorption rate is comparatively low; thus it was chosen as the proper thickness. The relevant absolute radioactivity, surface power, and self-absorption rate were 0.101121 Ci, 3.38845 μW, and 67.470%, respectively.

The decay formula of ^{63}Ni is $^{63}_{28}\mathrm{Ni} \rightarrow {}^{63}_{29}\mathrm{Cu} + e^{-} + \bar{\nu}_{e}$. Eventually, the ^{63}Ni source changes into a mixture of ^{63}Ni and ^{63}Cu. In this process, the product ^{63}Cu is also solid, and there are no other reactions that cause decrease in the radioactivity. For the 2.00337 μm ^{63}Ni source mentioned above, the changes of time-related surface power and self-absorption rate are shown in Fig. 2b. As time goes by, the surface power-decline approximately follows the exponential decay law, while the self-absorption rate rises slightly. This is because ^{63}Ni and its decay product ^{63}Cu have almost the same density, and the difference in their atomic numbers is very small, which means it has little effect on the regular pattern of surface power decrease. The rise of the self-absorption rate is caused by a rise in the average electron number.

5 Choice of metals for Schottky and Ohmic contacts

For this work, n-type ZnO was selected to obtain the theoretical electrical behavior of Schottky devices because the fabrication of n-type ZnO is easier, and there are more studies about Schottky barriers on n-type ZnO. The influence of the surface state is neglected in the simulation. Theoretically, when a metal is brought into intimate contact with a semiconductor, whether it is an Ohmic or Schottky contact is defined by the work function of the metal and electron affinity of the semiconductor [39]. This can be expressed by the Schottky–Mott rule [44]:

Table 1 Densities, work functions of metals, and ideal barrier heights of n-type ZnO

Metal	Al	Ag	Ti	Au	Pd	Ni	Pt
Density/g cm^{-3}	2.7	10.5	4.51	19.32	12.02	8.9	21.45
ϕ_m (eV)	4.28	4.26	4.33	5.1	5.12	5.15	5.64
ϕ_B (eV)	0.18	0.16	0.23	1.0	1.02	1.05	1.54

$$\phi_B = \phi_m - \chi. \quad (2)$$

This form is only available for Schottky barriers formed on n-type semiconductors, where ϕ_B is the Schottky barrier height, which is defined as the difference in electrical potential between the Fermi energy of the metal and the band edge where the majority carrier resides. The term ϕ_m is the metal work function, which is the energy needed to move an electron from the Fermi level to vacuum. Here, χ is the electron affinity of n-type ZnO (4.1 eV), which is the difference in potential between the conduction band edge and the vacuum level. The densities, work functions of metals, and ideal Schottky barrier heights are presented in Table 1. To form a Schottky contact, the Schottky barrier height should be larger, and the doping concentration should be lower, than in the conduction band or valence band density of states. For n-type ZnO, metals with higher ϕ_m are appropriate (i.e., Au, Pd, Ni, and Pt) and the conduction band density of states limits the doping concentration.

Table 1 can also be used to select metals to produce electrodes. Another metal–semiconductor contact, namely the Ohmic contact (which has relatively low contact resistance to the semiconductor bulk or series resistance), is appropriative for fabricating electrodes. In an actual Ohmic contact with gratifying performance, there should not be

obvious performance degradation of devices, and the voltage drop should be negligible in relation to the drop across the device's active region. An ideal Ohmic contact is formed when the barrier is zero, and in this condition the carriers are free to flow in or out of the semiconductor to ensure that the contact has minimum resistance [39]. For an n-type ZnO, the work function of the selected metal should be close to or smaller than the electron affinity of ZnO. It can be seen that Al, Ag, and Ti have relatively low work functions, indicating that they are adequate for this kind of contact. To form an Ohmic contact on ZnO with low contact resistivity, increase in the ZnO surface doping concentration is beneficial, along with reducing the Schottky barrier height. By applying these two methods, the barrier width becomes very thin, and the carriers are able to tunnel through.

6 Energy deposition

The simulation model is presented in Fig. 3. ZnO bulk ($1 \times 1 \times 0.5$ cm^3) was utilized for energy deposition. In this model, a layer of 200 nm is presented that refers to the dead layer (in which the deposited energy cannot be utilized). This includes the p-type region for the PN junction and metal layer for the Schottky diodes. The source was set on the bottom surface of the dead layer, and all particles were vertically incident. The energy deposition at initiation (time zero) in the dead layer and effective area (from the upper surface of the metal layer/p-type ZnO layer to the area of stratification) are presented in Fig. 4a. For all kinds of devices, more than 99% of the energy was deposited 6 μm from the upper surface of the source to the stratification area; therefore, the effective area was set. To utilize fully the energy produced, the width of the depletion layer was set at the same thickness as the effective area, which was 5.8 μm. Within the dead layer, the energy deposition remained almost unchanged throughout the simulations. Figure 4b shows the change of time-related energy deposition, which has a slight downward trend in both the effective area and the dead layer.

The energy deposition comparisons of Schottky diodes and PN junctions are also shown in Fig. 4. In the dead layer, energy deposition takes the order $E_{Pt} > E_{Au} > E_{Pd} > E_{Ni} > E_{ZnO}$, while in the effective area, the situation is completely opposite. Clearly, from the energy deposition point of view, Ni is the most suitable metal for a Schottky diode among these four metals because it has relatively lower density (shown in Table 1). This leads to less energy deposited in the metal itself and more in the effective area. Moreover, a ZnO homojunction has the most energy deposition in the effective area among all these devices because ZnO has the lowest density (5.6 g/cm^3).

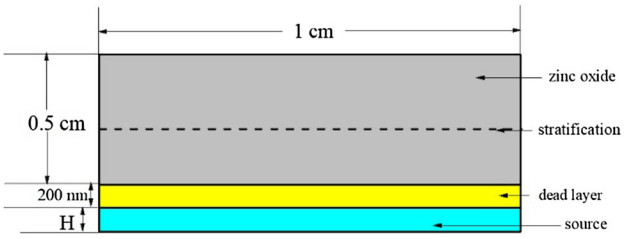

Fig. 3 Energy deposition model (Color online)

7 Analyses of built-in potential and depletion width in Schottky diodes and PN junctions

In a betavoltaic battery, electron–hole pairs are separated by the potential built into the depletion region. To exploit the beta source energy, the depletion width and the energy deposition range should be well matched. The depletion width can be changed by adjusting the doping concentrations. For Schottky diodes, the built-in potential is given by the following relation [20]:

$$V_{bi} = \phi_B - V_t \ln \frac{N_c}{N_D}, \tag{3}$$

where V_t is the thermal voltage, and $V_t = 0.0259$ V at ambient temperature. Here, N_c is the conduction band effective density of states, and N_D is the doping concentration of n-type ZnO (cm^{-3}).

At zero bias, the depletion width is given by [20]:

$$W = \sqrt{\frac{2\varepsilon_s \varepsilon_0 \phi_i}{qN_D}}, \tag{4}$$

where ε_s is 8.75, the relative permittivity of ZnO, ε_0 is the vacuum permittivity, and q is the electron charge.

In equilibrium condition, the built-in potential for PN junctions is given by the following relation [45]:

$$V_{bi} = V_t \cdot \ln\left(\frac{N_A N_D}{n_i^2}\right). \tag{5}$$

Here, N_A and N_D are doping concentrations of the p- and n-types (cm^{-3}). At normal atmospheric temperature, they approximate the carrier intensities, and n_i is the intrinsic carrier concentration.

The depletion width of a PN junction can be calculated using [45]:

$$W = \sqrt{\frac{2\varepsilon_s \varepsilon_0}{q} \cdot \left(\frac{N_A + N_D}{N_A N_D}\right) V_{bi}}. \tag{6}$$

Theoretically, the intrinsic carrier concentration can be expressed by:

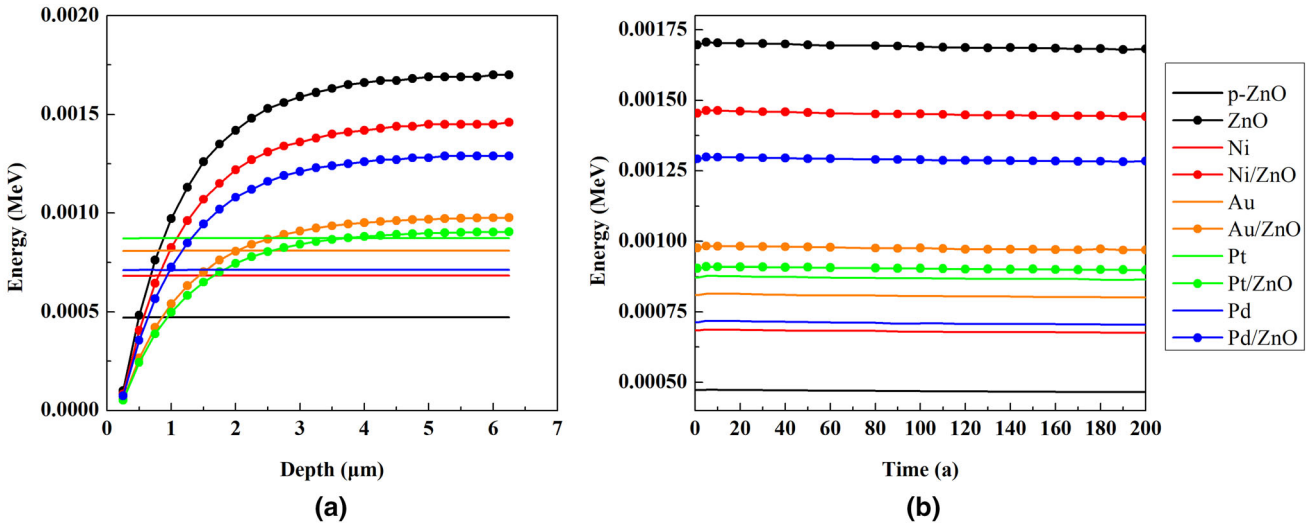

Fig. 4 Energy deposition in each device: **a** at initiation (time zero) and **b** time-related energy deposition with effective area of 5.8 μm (Color online)

$$n_i = (N_c N_v)^{1/2} \exp\left(-\frac{E_g}{2k_0 T}\right). \quad (7)$$

The term E_g is the bandgap of ZnO, and N_c and N_v are effective state densities of the conduction and valence bands, which can be calculated using

$$N_c = 2\frac{\left(2\pi m_n^* k_0 T\right)^{3/2}}{h^3} \quad \text{and} \quad N_v = 2\frac{\left(2\pi m_p^* k_0 T\right)^{3/2}}{h^3},$$

where m_n^* and m_p^* indicate the effective masses of electrons and holes, k_0 indicates the Boltzmann constant, and T *is* the absolute temperature. In ZnO material, m_n^* and m_p^* are 0.27 m_0 and 0.64 m_0, respectively [46]. It was determined that $N_c = 3.52 \times 10^{18}$ cm^{-3}, $N_v = 1.28 \times 10^{19}$ cm^{-3}, and $n_i = 3.74 \times 10^{-10}$ cm^{-3}. These equations are only adequate for non-degenerate semiconductors ($N_D \ll N_c$ and $N_A \ll N_v$). Thus, for ZnO material, N_D and N_A should be no more than 1×10^{18} and 5×10^{18} cm^{-3}, respectively. The m_n^* and m_p^* selected here are a little different from those in our previous work, because we had to match the universally acknowledged value of the effective Richardson's constant of ZnO [46] (that is, 32 A cm^{-2} K^{-2} while $m_n^* = 0.27\ m_0$). These differences led to small changes in the values of N_c and N_v; nonetheless, the doping concentration ranges for non-degenerate semiconductors remained the same.

In this work, the depletion width was 5.8 μm. For Schottky diodes, the relationships of V_{bi} and W versus N_D are shown in Fig. 5a. With increase in the doping concentration, the built-in potential increases slightly while the depletion width decreases substantially. For the PN junctions, N_D was set at 10^{16} cm^{-3}, and the relationships of V_{bi} and W versus N_A are shown in Fig. 5b. These resemble the regular pattern of a Schottky diode. The selected doping concentrations and built-in potentials are listed in Table 2.

8 Electrical performance simulations

In the following calculations, it was assumed that the electron–hole pairs in the depletion region are completely collected, and that outside this region, none of them are collected. With these assumptions, the short-circuit current can be expressed by the following equation [45]:

$$I_{SC} = \frac{Aq}{E_{e-h}} \cdot \sum_{n=1}^{n} \mathrm{CE}(n) \times E(n), \quad (8)$$

where CE(n) is the collection rate of electron–hole pairs in layer n of the sample, $E(n)$ is the deposition energy in layer n, A is the absolute radioactivity, q is the electron charge, and E_{e-h} is the average ionization threshold. In Sect. 6, we obtained the energy deposition in the depletion region, $E(n)$, and according to the condition above, the relevant CE(n) was 1.

In our previous work, we used an empirical equation to estimate E_{e-h} because the universally acknowledged value was not presented [47]:

$$E_{e-h} = 2.8E_g + 0.5, \quad (9)$$

where E_g is the bandgap and E_{e-h} as achieved was 9.9 eV.

To evaluate device quality, reverse saturation current is often utilized. If a device has low reverse saturation, it has fine quality. For Schottky diodes, the density of a reverse saturation current (A/cm^2) can be expressed by [20]:

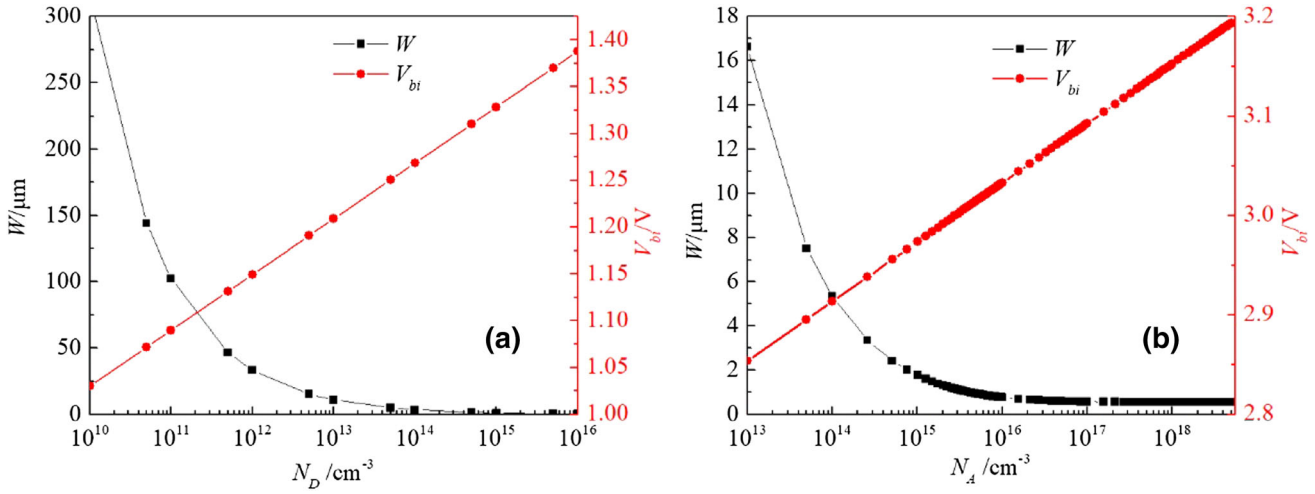

Fig. 5 Relations between built-in potential, depletion width, and doping concentration: **a** Pt/ZnO Schottky contact and **b** PN junction (with N_D set as 10^{16} cm^{-3}) (Color online)

Table 2 Selected doping concentrations and built-in potentials

	PN junction	Pt/ZnO	Au/ZnO	Ni/ZnO	Pd/ZnO
Doping concentrations ($\times 10^{13}$ cm^{-3})	$N_D = 10^3$ $N_A = 8.44$	$N_D = 3.57447$	$N_D = 1.9765$	$N_D = 2.1258$	$N_D = 1.8978$
Built-in potential (V)	2.90913	1.24224	0.68690	0.73878	0.70585

$$J_0 = A^* T^2 \exp(-\phi_B/V_t), \tag{10}$$

where A^* is the effective Richardson's constant. For ZnO, the universally acknowledged value is $m_n^* = 0.27\ m_0$, A^* is 32 A cm^{-2} K^{-2}. For PN junctions, it can be determined by [47]:

$$J_0 = 1.5 \times 10^5 \exp(-E_g/k_0 T), \tag{11}$$

where k_0 indicates the Boltzmann constant.

The open-circuit voltage can be obtained by the following formula:

$$V_{oc} = \frac{nk_0 T}{q} \ln\left(1 + \frac{J_{sc}}{J_0}\right), \tag{12}$$

where n is the ideal factor. In this work, it is considered to be 1, which indicates an ideal PN junction or Schottky device. Here, J_{sc} is the short-circuit current density.

One of the key parameters that evaluates the performance of a betavoltaic battery is the fill factor (FF). A battery with higher fill factor has output power that comes closer to its theoretical maximum, thus its efficiency is higher. The definition of the fill factor is the ratio of the maximum output power (P_m) to the product of the relative open-circuit voltage (V_{oc}) and the short-circuit current (I_{sc}):

$$\mathrm{FF} = \frac{P_m}{V_{oc} \cdot I_{sc}}. \tag{13}$$

To evaluate the fill factor, an empirical equation can be utilized [47]:

$$\mathrm{FF} = \frac{v_{oc} - \ln(v_{oc} + 0.72)}{v_{oc} + 1}, \tag{14}$$

where $v_{oc} = V_{oc}/(k_0 T/q)$.

The definition of maximum output power is as follows [47]:

$$P_m = \mathrm{FF} \times V_{oc} \times I_{sc}. \tag{15}$$

In this work, we used the device converting efficiency to evaluate the total performance of the betavoltaic battery, which can be defined as below [48]:

$$\eta = \frac{P_m}{P_{source}}, \tag{16}$$

where P_{source} is the surface power of the source.

9 Results and discussion

According to Eqs. (10) and (11), the short-circuit current densities are constants without time-related changes, in theory. The short-circuit current densities for a ZnO-based

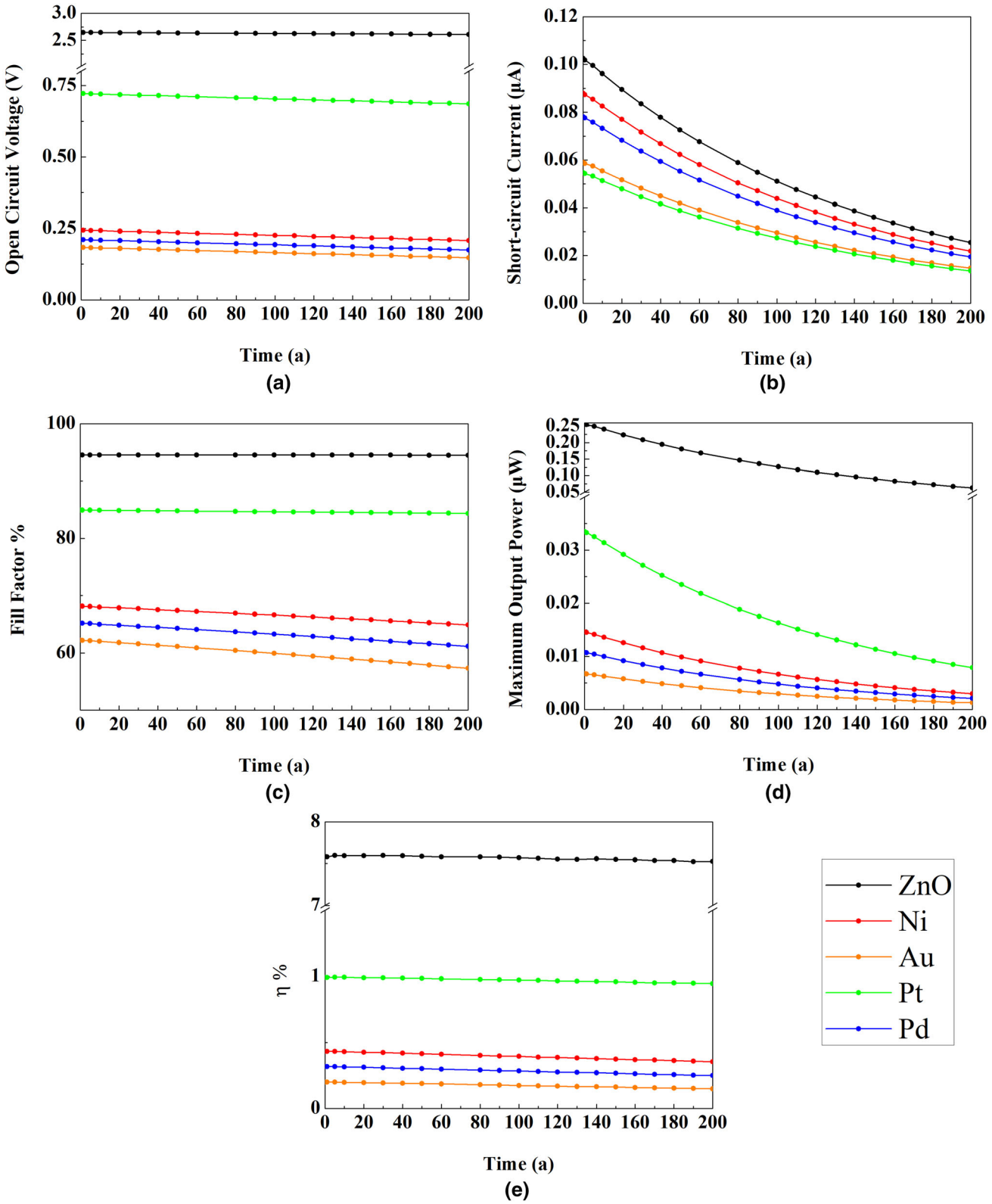

Fig. 6 Time-related electrical properties: **a** V_{oc}, **b** I_{sc}, **c** FF, **d** P_m, and **e** conversion efficiency (Color online)

PN junction and for Pt, Au, Pd, and Ni/ZnO Schottky diodes are 4.65055×10^{-52}, 4.32989×10^{-20}, 4.91208×10^{-11}, 2.26936×10^{-11}, and 7.12622×10^{-12} A/cm^2, respectively. These current densities indicate that the PN junction has the best quality among all these devices, while the Pt/ZnO Schottky device has the best quality among the Schottky devices.

Time-related electrical properties of the PN junction and of Schottky diodes are presented in Fig. 6a–e. At the start (time zero), the ZnO-based PN junction has the highest open-circuit voltage, short-circuit current, fill factor, maximum output power, and conversion efficiency (up to 2.64452 V, 0.10259 μA, 94.5366%, 0.25647 μW, and 7.584%, respectively). These are much higher than with other Schottky devices. The reason is that the PN junction has very low reverse saturation current density, which leads to relatively higher V_{oc} according to Eq. (12). Meanwhile, the density of ZnO is lower than all the Schottky metals mentioned above, leading to more energy deposition in the effective area. Among these Schottky diodes, the Pt/ZnO device has the highest V_{oc}, P_m, FF, and η due to its highest ϕ_m, which leads to the highest ϕ_B and lowest J_0. In addition, the Ni/ZnO device has the largest I_{sc} because Ni has the smallest atomic number and density among all the selected metals, which lead to the most energy deposition in the effective area.

All the electrical properties (in a battery) decline as time goes by. The declines of I_{sc} and P_m follow the exponential law, while the declines of V_{oc}, FF, and η show approximately linear patterns. Among all the electrical properties, the decline of P_m is the most evident. Hence, P_m was selected to evaluate the validity of the battery concept. Taking the ZnO-based PN junction as an example, in 200 years the decline rates of V_{oc}, I_{sc}, P_m, FF, and η would be 1.365, 75.189, 0.065, 75.544, and 0.748%, respectively. While for Pt, Au, Pd, and Ni/ZnO Schottky diodes, the decline of P_m becomes more evident (76.523, 81.589, 80.636, and 79.862%, respectively). Thus, from the viewpoint of long-term service, Pt/ZnO and Ni/ZnO Schottky devices are more suitable than PN junctions, whereas Au/ZnO and Pd/ZnO Schottky devices are less adaptable. A Pt/ZnO Schottky diode could be utilized in devices that need high V_{oc} and P_m, and a Ni/ZnO Schottky diode would be more suitable for devices needing higher electric current.

In short, irrespective of whether the time factor is considered or not, PN junctions have the highest V_{oc}, I_{sc}, P_m, FF, and η (that is, the best electrical performance) among all the competitors discussed here. Regardless of long-term radiation damage, PN junction-based devices also have the longest active period. Nevertheless, Schottky diodes have their own advantages. The fabrication of Schottky diodes requires only one type of extrinsic semiconductor, which is very convenient for semiconductors with asymmetry doping problems (i.e., for GaN and ZnO obtaining n-type semiconductors is easier, while for diamond it is easier to get p-type ones). Compared with PN junction-based devices, Schottky diodes offer additional choices of state-of-the-art semiconductors, and the manufacturing processes are simpler. When fabricating Schottky diode-based betavoltaic batteries, the radiation source is in contact with the metal layer of the Schottky diode, which makes it less susceptible to radiation damage. In contrast, with a PN junction, the semiconductor lattice is prone to displacement due to radiation damage, because the radiation source is in direct contact with the semiconductor. All of these advantages indicate that Schottky diodes are a good alternative to PN junction-based betavoltaic batteries.

10 Conclusion

In summary, Schottky contacts using different metals for n-type ZnO and ZnO-based PN junctions were utilized as energy converting structures for betavoltaic batteries, with 0.101121 Ci ^{63}Ni as the selected beta source. Based on Monte Carlo simulations, the time-related self-absorption rate and electrical properties of a number of devices were obtained and compared. For a ^{63}Ni source, the self-absorption rate showed a slightly upward trend as time went by. The optimal doping concentration for Schottky diodes was $N_D = 1.9765–3.57447 \times 10^{13}$ cm^{-3}, and for PN junctions it was $N_A = 8.44 \times 10^{13}$ cm^{-3} while $N_D = 10^{16}$ cm^{-3}. Generally, the electrical performance of PN junctions is better than that of Schottky diodes. Among all the kinds of Schottky diodes discussed here, Pt/ZnO has the highest maximum output power, and Ni/ZnO has the greatest short-circuit current. Taking long-term service into consideration, Pt/ZnO and Ni/ZnO are the most suitable among the Schottky diodes. A Pt/ZnO Schottky diode could be utilized in devices needing high open-circuit voltage and maximum output power, while a Ni/ZnO Schottky diode would be more suitable for devices needing greater electrical current. Although its electrical performance is relatively inferior, the ZnO-based Schottky diode has its own advantages, including easier fabrication, independence of p-type ZnO, and more resistance to radiation damage. Therefore, they still are considered viable alternatives to PN junctions as the energy converting structures of betavoltaic batteries.

References

1. R. Ramesham, Fabrication of diamond microstructures for microelectromechanical systems (MEMS) by a surface

micromachining process. Thin Solid Films **340**, 1–6 (1999). https://doi.org/10.1016/s0040-6090(98)01370-4
2. Loughborough University, *An Introduction to MEMS (Microelectromechanical Systems)* (PRIME Faraday Partnership, Loughborough, 2002)
3. X.Y. Li, Y. Ren, X.J. Chen et al., 63Ni schottky barrier nuclear battery of 4H-SiC. J. Radioanal. Nucl. Chem. **287**, 173–176 (2011). https://doi.org/10.1007/s10967-010-0746-7
4. T.R. Alam, M.A. Pierson, Principles of betavoltaic battery design. J. Energy Power Sour. **3**, 11–41 (2016)
5. S. Kumar, Atomic batteries: energy from radioactivity. J. Nucl. Energy Sci. Power Gener. Technol. **05**, 1–8 (2015). https://doi.org/10.4172/2325-9809.1000144
6. W.G. Pfann, W. Van Roosbroeck, Radioactive and photoelectric p-n junction power sources. J. Appl. Phys. **25**, 1422–1434 (1954). https://doi.org/10.1063/1.1721579
7. W. Ehrenberg, C.-S. Lang, R. West, The electron voltaic effect. Proc. Phys. Soc. Sect. A **64**, 424 (1951). https://doi.org/10.1088/0370-1298/64/4/109
8. P. Rappaport, The electron-voltaic effect in p-n junctions induced by beta-particle bombardment. Phys. Rev. **93**, 246–247 (1954). https://doi.org/10.1103/physrev.93.246.2
9. K.A. Rosenkranz, Clinical experience with nuclear-powered pacemakers (Promethium-147) in *Engineering in Medicine* (Springer, Berlin, 1975), pp. 503–529. https://doi.org/10.1007/978-3-642-66187-7_31
10. A.J. Martinis, Initial U. S. experience with promethium-147 fueled cardiac pacemakers, in *Engineering in Medicine* (Springer Berlin, 1975), pp. 531–538. https://doi.org/10.1007/978-3-642-66187-7_32
11. V. Bormashov, S. Troschiev, A. Volkov et al., Development of nuclear microbattery prototype based on Schottky barrier diamond diodes. Phys. Status Solidi Appl. Mater. Sci. **212**, 2539–2547 (2015). https://doi.org/10.1002/pssa.201532214
12. S. Theirrattanakul, M. Prelas, A methodology for efficiency optimization of betavoltaic cell design using an isotropic planar source having an energy dependent beta particle distribution. Appl. Radiat. Isot. **127**, 41–46 (2017). https://doi.org/10.1016/j.apradiso.2017.05.005
13. J. Russo, M. Litz, W. Ray et al., Development of tritiated nitroxide for nuclear battery. Appl. Radiat. Isot. **125**, 66–73 (2017). https://doi.org/10.1016/j.apradiso.2017.04.013
14. Y.P. Liu, Z.H. Xu, H. Wang et al., Vacuum degree effects on betavoltaics irradiated by 63Ni with differently apparent activity densities. Sci. China Technol. Sci. **60**, 282–288 (2017). https://doi.org/10.1007/s11431-016-0505-x
15. A.V. Gurskaya, M.V. Dolgopolov, V.I. Chepurnov, C-14 beta converter. Phys. Part. Nucl. **48**, 941–944 (2017). https://doi.org/10.1134/s106377961706020x
16. H. Guo, H. Yang, Y. Zhang, Betavoltaic microbatteries using porous silicon. Paper presented at IEEE 20th International Conference on Micro Electro Mechanical Systems (MEMS) (2007). https://doi.org/10.1109/memsys.2007.4433006
17. Q. Zhang, N. Wang, P. Zhou, et al., A betavoltaic microbattery using zinc oxide nanowires under build in potential difference. Paper presented at Proceedings of the IEEE International Conference on Micro Electro Mechanical Systems (MEMS) (2016). https://doi.org/10.1109/memsys.2016.7421846
18. X. Tang, D. Ding, Y. Liu, D. Chen, Optimization design and analysis of Si-63Ni betavoltaic battery. Sci. China Technol. Sci. **55**, 990–996 (2012). https://doi.org/10.1007/s11431-012-4752-6
19. L.C. Olsen, Review of betavoltaic energy conversion. Paper Presented at Space Photovoltaic Research and Technology Conference (1993)
20. D.Y. Qiao, X.J. Chen, Y. Ren, W.Z. Yuan, A micro nuclear battery based on SiC schottky barrier diode. J. Microelectromech. Syst. **20**, 685–690 (2011). https://doi.org/10.1109/jmems.2011.2127448
21. C. Han, X.Z. Cui, X.H. Liang et al., Study of the characteristics of an irradiated 4H-SiC charge particle detector. Nucl. Tech. **42**(5), 050501 (2019). https://doi.org/10.11889/j.0253-3219.2019.hjs.42.050501. **(in Chinese)**
22. M. Huang, R. Li, D.M. Li et al., Research and application of silicon carbide diode in high voltage power supply. Nucl. Tech. **42**(5), 050402 (2019). https://doi.org/10.11889/j.0253-3219.2019.hjs.42.050402. **(in Chinese)**
23. C.E. Munson, Q. Gaimard, K. Merghem et al., Modeling, design, fabrication and experimentation of a GaN-based, ^{63}Ni betavoltaic battery. J. Phys. D Appl. Phys. **51**, 035101 (2018). https://doi.org/10.1088/1361-6463/aa9e41
24. Z. Cheng, H. San, Y. Li, X. Chen, The design optimization for GaN-based betavoltaic microbattery. Paper presented at IEEE 5th International Conference on Nano/Micro Engineered and Molecular Systems, NEMS (2010). https://doi.org/10.1109/nems.2010.5592469
25. S. Tarelkin, V. Bormashov, E. Korostylev et al., Comparative study of different metals for Schottky barrier diamond betavoltaic power converter by EBIC technique. Phys. Status Solidi Appl. Mater. Sci. **213**, 2492–2497 (2016). https://doi.org/10.1002/pssa.201533060
26. F. Rahmani, H. Khosravinia, Optimization of silicon parameters as a betavoltaic battery: comparison of Si p-n and Ni/Si Schottky barrier. Radiat. Phys. Chem. **125**, 205–212 (2016). https://doi.org/10.1016/j.radphyschem.2016.04.012
27. D.C. Look, D.C. Reynolds, J.W. Hemsky et al., Production and annealing of electron irradiation damage in ZnO. Appl. Phys. Lett. **75**, 811–813 (1999). https://doi.org/10.1063/1.124521
28. F. Xiu, J. Xu, P.C. Joshi, et al., ZnO doping and defect engineering: a review, in *Semiconductor Materials for Solar Photovoltaic Cells*. (Springer Cham, 2016), pp. 105–140. https://doi.org/10.1007/978-3-319-20331-7_4
29. A. Janotti, C.G. Van De Walle, Fundamentals of zinc oxide as a semiconductor. Rep. Prog. Phys. **72**, 126501 (2009). https://doi.org/10.1088/0034-4885/72/12/126501
30. Y. Lei, Y. Yang, Y. Liu et al., The radiation damage of crystalline silicon PN diode in tritium beta-voltaic battery. Appl. Radiat. Isot. **90**, 165–169 (2014). https://doi.org/10.1016/j.apradiso.2014.03.027
31. D.E. Meier, A.Y. Garnov, J.D. Robertson et al., Production of 35S for a liquid semiconductor betavoltaic. J. Radioanal. Nucl. Chem. **282**, 271–274 (2009). https://doi.org/10.1007/s10967-009-0157-9
32. V. Avrutin, D.J. Silversmith, H. Morkoc, Doping asymmetry problem in ZnO: current status and outlook. Proc. IEEE **98**, 1269–1280 (2010). https://doi.org/10.1109/jproc.2010.2043330
33. J.G. Lu, Y.Z. Zhang, Z.Z. Ye et al., Low-resistivity, stable p-type ZnO thin films realized using a Li-N dual-acceptor doping method. Appl. Phys. Lett. **88**, 222114 (2006). https://doi.org/10.1063/1.2209191
34. J.J. Yang, Q.Q. Fang, W.H. Du et al., High mobility ultrathin ZnO p-n homojunction modulated by Zn0.85Mg0.15O quantum barriers. Chin. Phys. B. **27**, 1–5 (2018). https://doi.org/10.1088/1674-1056/27/3/037804
35. J.J. Yang, Q.Q. Fang, D.D. Wang et al., The ZnO p-n homojunctions modulated by ZnMgO barriers. AIP Adv. **5**, 047104 (2015). https://doi.org/10.1063/1.4917178
36. X. Yang, X. Xu, F. Liu et al., Fabrication of p-ZnO:Na/n-ZnO:Na homojunction by surface pulsed laser irradiation. RSC Adv. **7**, 37296–37301 (2017). https://doi.org/10.1039/c7ra05574a
37. L. Qi, Z. Chai, H. Yang et al., A facile and reproducible synthesis of non-polar ZnO homojunction with enlarged rectification rate

and colorful light emission. J. Alloys Compd. **793**, 295–301 (2019). https://doi.org/10.1016/j.jallcom.2019.04.109
38. R. Yatskiv, S. Tiagulskyi, J. Grym et al., Electrical and optical properties of rectifying ZnO homojunctions fabricated by wet chemistry methods. Phys. Status Solidi Appl. Mater. Sci. **215**, 1–6 (2018). https://doi.org/10.1002/pssa.201700592
39. L.J. Brillson, Y. Lu, ZnO Schottky barriers and Ohmic contacts. J. Appl. Phys. **109**, 121301 (2011). https://doi.org/10.1063/1.3581173
40. L. Agarwal, S. Tripathi, P. Chakrabarti, Analysis of structural, optical and electrical properties of metal/p-ZnO-based Schottky diode. J. Semicond. **38**, 104002 (2017). https://doi.org/10.1088/1674-4926/38/10/104002
41. G. Lutz, *Semiconductor Radiation Detectors* (Springer, Berlin, 2007). https://doi.org/10.1007/978-3-540-71679-2
42. Y. Liu, R. Hu, Y. Yang et al., Investigation on a radiation tolerant betavoltaic battery based on Schottky barrier diode. Appl. Radiat. Isot. **70**, 438–441 (2012). https://doi.org/10.1016/j.apradiso.2011.10.013
43. M.A. Prelas, C.L. Weaver, M.L. Watermann et al., A review of nuclear batteries. Prog. Nucl. Energy **75**, 117–148 (2014). https://doi.org/10.1016/j.pnucene.2014.04.007
44. L. Fang, J.X. Dong, S.F. Zhang et al., Latest progress of schottky contacts fabricated on ZnO substrates. Chin. J. Vac. Sci. Technol. **28**, 126–132 (2007). **(in Chinese)**
45. X. Tang, Y. Liu, D. Ding, D. Chen, Optimization design of GaN betavoltaic microbattery. Sci. China Technol. Sci. **55**, 659–664 (2012). https://doi.org/10.1007/s11431-011-4739-8
46. D. Somvanshi, S. Jit, Mean barrier height and Richardson constant for Pd/ZnO Thin film-based Schottky diodes grown on n-Si substrates by thermal evaporation method. IEEE Electron Device Lett. **34**, 1238–1240 (2013). https://doi.org/10.1109/led.2013.2278738
47. Y.P. Liu, X.B. Tang, Z.H. Xu et al., Influences of planar source thickness on betavoltaics with different semiconductors. J. Radioanal. Nucl. Chem. **304**, 517–525 (2015). https://doi.org/10.1007/s10967-014-3879-2
48. Y.M. Liu, J. Bin Lu, X.Y. Li et al., Theoretical prediction of diamond betavoltaic batteries performance using 63Ni. Chin. Phys. Lett. **35**, 5–9 (2018). https://doi.org/10.1088/0256-307x/35/7/072301